Electronic Supplementary Information for:

A One-Dimensional Coordination Polymer Exhibiting Simultaneous Spin-Crossover and Semiconductor Behaviours

Wei Xue,[a] Bao-Ying Wang,[a] Jie Zhu,[a] Wei-Xiong Zhang,[a] Yue-Biao Zhang,[a] Hai-Xia Zhao[b] and Xiao-Ming Chen*[a]

[a] *MOE Laboratory of Bioinorganic and Synthetic Chemistry, State Key Laboratory of Optoelectronic Materials and Technologies, School of Chemistry & Chemical Engineering, Sun Yat-Sen University, Guangzhou 510275, P.R. China. E-mail: cxm@mail.sysu.edu.cn*
[b] *State Key Laboratory of Physical Chemistry of Solid Surface and College of Chemistry and Chemical Engineering, Xiamen University, Xiamen 361005, P.R. China.*

Experimental Section

Synthesis of **1**: $Co(OAc)_2 \cdot 4H_2O$ (0.025 g, 0.1 mmol) was added to a well stirred solution of 8-mercaptoquinoline sodium salt (0.037 g, 0.2 mmol) in ethanol (8 ml) with acetic acid (0.1 ml). The suspension was then sealed in a 12-ml Teflon-lined stainless steel autoclave and heated to 160 °C for 3 days. Upon cooling down to room temperature at a rate of 5 °C /hr, needle-like black crystals were obtained. (0.022 g, 57.9%). Elemental analysis (%) calcd for 1: C 56.99, H 3.19, N 7.38, S 16.91; found: C 56.74, H 3.39, N 7.29, S 16.87.

The intensity data of **1** were recorded on a Bruker SMART Apex CCD system with Mo Kα radiation (λ = 0.71073 Å) at 272(2) K. The structure was solved by direct methods and refined by full-matrix least-squares technique on F^2 using SHELXTL. CCDC reference numbers 799875-799881 contains the crystallographic data for this paper. These data can be obtained free of charge *via* www.ccdc.cam.ac.uk (or from the Cambridge Crystallographic Data Centre, 12 Union Road, Cambridge CB21EZ, UK; fax: (+44)1223-336-033; or deposit@ccdc.cam.ac.uk).

Magnetic susceptibility measurements on **1** were performed with a Quantum Design MPMS-XL7 SQUID. Data were corrected for the diamagnetic contribution calculated from Pascal constants. Electrical conductivity was carried out with a Wayne Kerr 6500B Precision impendence analyzer. Optical reflectivity measurements were collected using a UV-Vis-NIR Spectrophotometer (UV-3150).

Simulation of the magnetic properties of 1: To simulate the magnetic properties of **1**, the molar fraction of Co^{II} ions in the high spin state, $x_{S=3/2}$, may be written by Equation (a),

$$x_{S=3/2} = \frac{1}{1+\exp\left[n\frac{\Delta H}{R}\left(\frac{1}{T}-\frac{1}{T_{1/2}}\right)\right]} \quad \text{(a)}$$

in which ΔH is the change in enthalpy between the high spin state and low spin state, R the gas constant, $T_{1/2}$ the spin transition temperature. The molar magnetic susceptibilities may then be expressed according to Equation (b),

$$\chi_M = (1-x_{S=3/2})\chi_{LS} + x_{S=3/2}\chi_{HS} \quad \text{(b)}$$

in which χ_{HS} and χ_{LS} are the molar magnetic susceptibilities for the high spin state and the low spin state, respectively. It follows that the molar magnetic susceptibilities at high spin state and low spin state may be estimated by a chain model according to Equation (c) and (d), respectively.

$$\chi_m T(T) = \frac{N_A \beta^2 g^2 S(S+1)}{3k}\frac{1+u}{1-u} \quad \text{(c)}$$

$$u = \coth\left[\frac{JS(S+1)}{kT}\right] - \left[\frac{kT}{JS(S+1)}\right] \quad \text{(d)}$$

Equation (e) is carried out for these considerations.

$$\chi_M T = (1-x_{S=3/2})\left[\frac{N_A \beta^2 g_{LS}{}^2 S_{LS}(S_{LS}+1)}{3k}\frac{1+u}{1-u}\right] + x_{S=3/2}\left[\frac{N_A \beta^2 g_{HS}{}^2 S_{HS}(S_{HS}+1)}{3k}\frac{1+u}{1-u}\right] \quad \text{(e)}$$

However, Equation (e) does not fit well to the experimental data. In this case, the simple phenomenological equation (f), where C_1+C_2 equals the Curie constant, and E_1, E_2 hold for "activation energies" was used to express molar magnetic susceptibilities.[10] The $\chi_M T$ can be written according to

$$\chi_M T = C_1 \exp(-E_1/kT) + C_2 \exp(-E_2/kT) \quad \text{(f)}$$

Equations (g), in which C_{LS}, E_{LS} for the antiferromagnetic exchange interaction at low spin Co^{II} ions,

$$\chi_M T = (1 - x_{S=3/2})\left[C_{LS}\exp(-E_{LS}/kT) + C_{LS'}\exp(-E_{LS'}/kT)\right] + x_{S=3/2}\left[C_{HS}\exp(-E_{HS}/kT) + C_{HS'}\exp(-E_{HS'}/kT)\right] \quad \text{(g)}$$

$C_{LS'}$, $E_{LS'}$ for the ferromagnetic exchange interaction at low spin state, C_{HS}, E_{HS} for the antiferromagnetic exchange interaction at high spin state and $C_{HS'}$, $E_{HS'}$ for the spin-orbital coupling of high spin Co^{II} ions.

Finally, the experimental data have been fitted in 26-340 K and are very well described according to Equation (g) (see Figure S3). Fitting the data in this range results in ΔH = 18.80 kJ·mol^{-1}, C_{HS} =0.67, $-E_{HS}/k$ = -23.87 cm^{-1}, $C_{HS'}$ =1.10, $-E_{HS'}/k$ = -54.28 cm^{-1}, C_{LS} =0.31, $-E_{LS}/k$ = -3.46 cm^{-1}, $C_{LS'}$ =0.10, $-E_{LS'}/k$ = 0.58 cm^{-1}, $T_{1/2}$=144.25 K. The value for $-E_{HS'}/k$ of -54.28 cm^{-1} is consistent with those giving in the literature for both the effects of spin-orbital coupling and site? distortion, while the value for $-E_{HS}/k$ of -23.87 cm^{-1} alludes to the overall antiferromagnetic exchange interaction.[15] As for the values estimated for the low spin state, $-E_{LS}/k$ of -3.46 cm^{-1} and $-E_{LS'}/k$ of 0.58 cm^{-1}, respectively, suggest the coexistence of antiferromagnetic and ferromagnetic coupling, while the domain exchange is antiferromagnetic. These results suggest the coexistence of spin-orbital coupling and strong antiferromagnetic exchange interaction at the high spin state and the canting-like behaviour at the low spin state.

Table S1. Crystal data and structure refinements for **1** at different temperatures.

Temperature (K)		112(2)	138(2)	165(2)	192(2)	218(2)	245(2)	272(2)
Empirical formula		C_{18} H_{12} Co N_2 S_2						
Wavelength (Å)		0.71073						
Crystal system		Monoclinic						
Space group		$P2_1/c$ (No. 14)						
Formula weight		379.37						
Unit-cell dimensions	*a*	3.6858(4)	3.6896(4)	3.6911(4)	3.6947(3)	3.6988(3)	3.7060(4)	3.7109(4)
	b	14.6127(15)	14.6443(15)	14.6918(14)	14.7215(13)	14.7379(12)	14.7577(14)	14.7647(14)
	c	12.8816(13)	12.9107(13)	12.9593(12)	12.9900(12)	13.0078(11)	13.0266(13)	13.0315(13)
	β	93.105(2)	92.903(2)	92.499(2)	92.2960(10)	92.2310(10)	92.207(2)	92.194(2)
Volume (Å^3)		692.78(12)	696.69(13)	702.10(12)	705.98(11)	708.55(10)	711.92(12)	713.48(12)
Z		2	2	2	2	2	2	2
Density (calcd. g/cm^3)		1.819	1.808	1.794	1.785	1.778	1.770	1.766
Absorption coeff. (mm^{-1})		1.538	1.529	1.518	1.509	1.504	1.497	1.493
F(000)		386	386	386	386	386	386	386
Crystal size (mm)		0.05 x 0.05 x 0.20						
Crystal color & shape		black, needle-like						
θ range data collection		2.1 to 26.0º	2.1 to 26.0º	2.1 to 26.0º	2.1 to 26.0º	2.1 to 26.0º	2.1 to 26.0º	2.1 to 26.0º
Reflections collected		3445	3483	3524	3539	3570	3552	3853
Independent reflections		1349	1357	1370	1373	1386	1285	1384
		R_{int} = 0.0159	R_{int} = 0.0227	R_{int} = 0.0132	R_{int} = 0.0139	R_{int} = 0.0140	R_{int} = 0.0128	R_{int} = 0.0137
Refinement method		Full-matrix least-square on F^2						
Data/restraints/parameters		1349/ 0/106	1357/ 0/106	1370/ 0/106	1373/ 0/106	1386/ 0/106	1385/0/106	1384/0/106
Goodness-of-fit on F^2		1.088	1.086	1.082	1.075	1.070	1.081	1.062
Final *R* indices [$I>2\sigma(I)$][a,b]		R_1 = 0.0274	R_1 = 0.0326	R_1 = 0.0269	R_1= 0.0271	R_1 = 0.0267	R_1 = 0.0266	R_1 = 0.0277
		wR_2 = 0.0784	wR_2 = 0.0915	wR_2 = 0.0758	wR_2 = 0.0761	wR_2 = 0.0751	wR_2 = 0.0755	wR_2 = 0.0836
R indices (all data)		R_1 = 0.0279	R_1 = 0.0334	R_1 = 0.0276	R_1 = 0.0277	R_1 = 0.0274	R_1 = 0.0274	R_1 = 0.0287
		wR_2 = 0.0789	wR_2 = 0.0923	wR_2 = 0.0764	wR_2 = 0.0767	wR_2 = 0.0757	wR_2 = 0.0760	wR_2 = 0.0851

[a] $R_1(F) = \Sigma||F_o| - |F_c||/\Sigma|F_o|$. [b] $wR_2(F^2) = [\Sigma\{w(F_o^2 - F_c^2)^2\}/\Sigma\{w(F_o^2)^2\}]^{0.5}$; $w^{-1} = \sigma^2(F_o^2) + (aP)^2 + bP$, where $P=[F_o^2 + 2F_c^2]/3$ and *a* and *b* are constants adjusted by the program.

Table S2. Selected interatomic and π–π interaction distances (Å) in **1**.

Temperature	Co-N	Co-S	Co-S'	π···π	Co···Co
112(2) K	1.9723(15)	2.2718(5)	2.7325(5)	3.337	3.686(1)
138(2) K	1.9953(16)	2.2940(5)	2.7234(5)	3.337	3.690(1)
165(2) K	2.0414(15)	2.3389(5)	2.6971(5)	3.328	3.691(1)
192(2) K	2.0661(15)	2.3629(5)	2.6874(5)	3.328	3.695(1)
218(2) K	2.0772(15)	2.3707(5)	2.6881(5)	3.329	3.699(1)
245(2) K	2.0831(15)	2.3756(5)	2.6939(5)	3.334	3.706(1)
272(2) K	2.0850(15)	2.3768(5)	2.6989(5)	3.338	3.711(1)

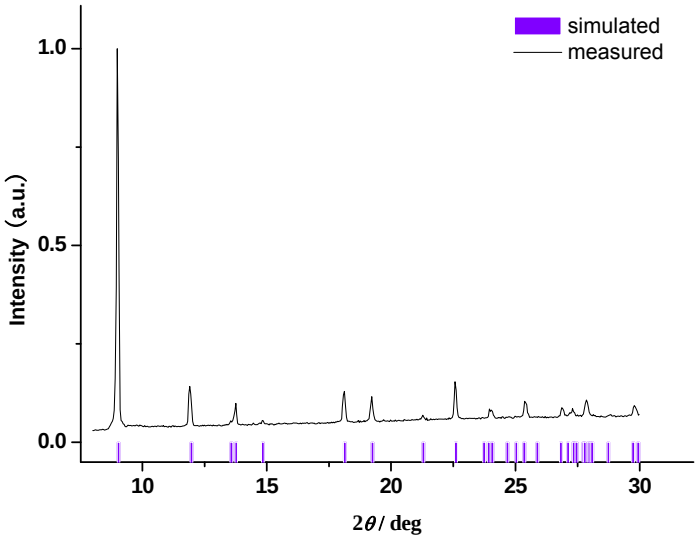

Figure S1. Measured (line) and simulated (bar) powder X-ray diffraction patterns of **1** at room temperature.

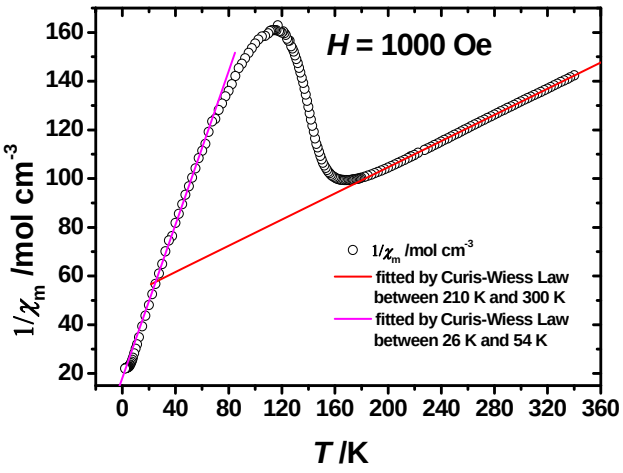

Figure S2. Inverse susceptibility 1/χ *vs*. temperature for **1.**

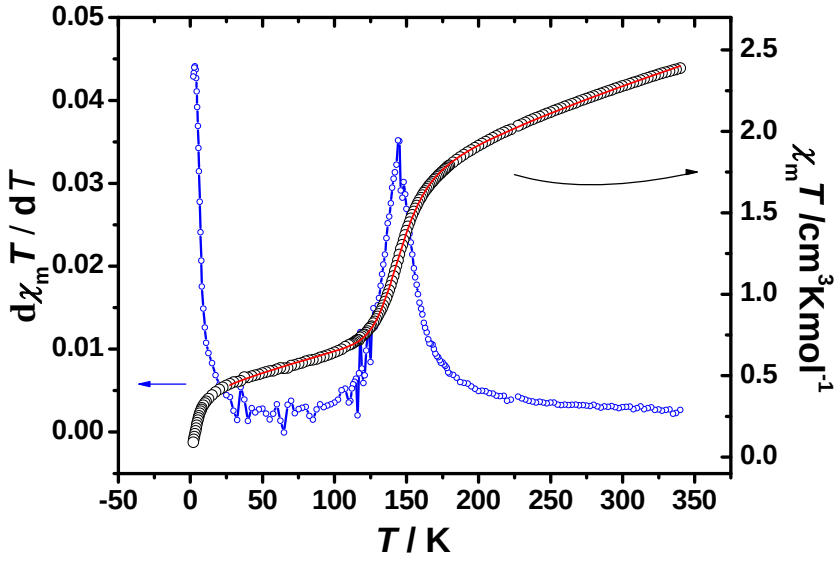

Figure S3. The temperature-dependent $\chi_M T$ at 10000 Gs (o), its derivative of temperature (blue line), and the best fit (red line) for **1**.

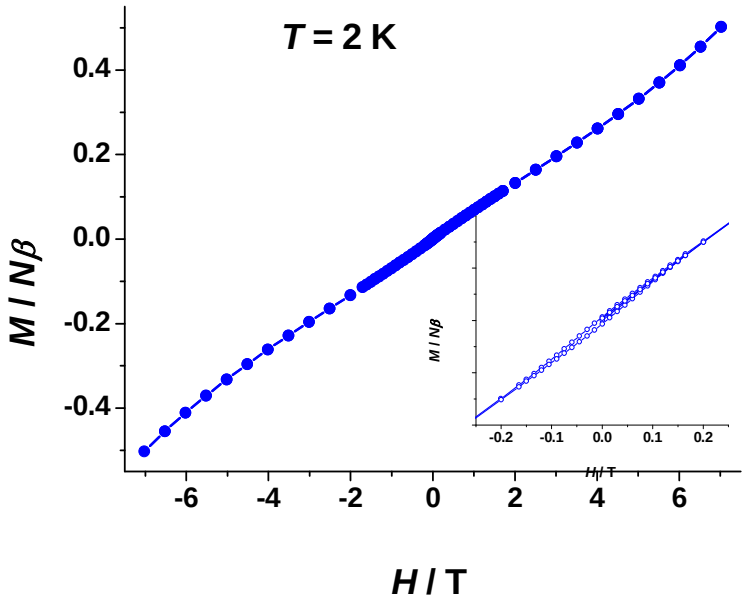

Figure S4. Hysteresis curves of **1** between –7 and +7 T at 2 K.

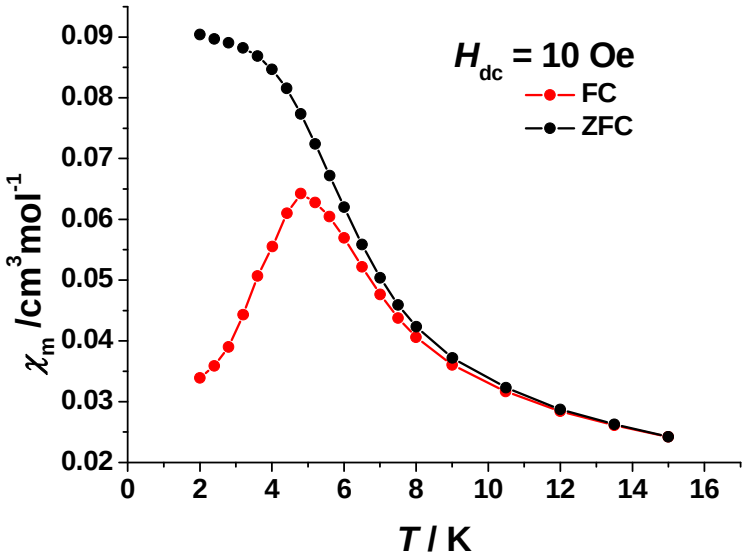

Figure S5. FC and ZFC magnetization of **1** measured at 10 Oe.

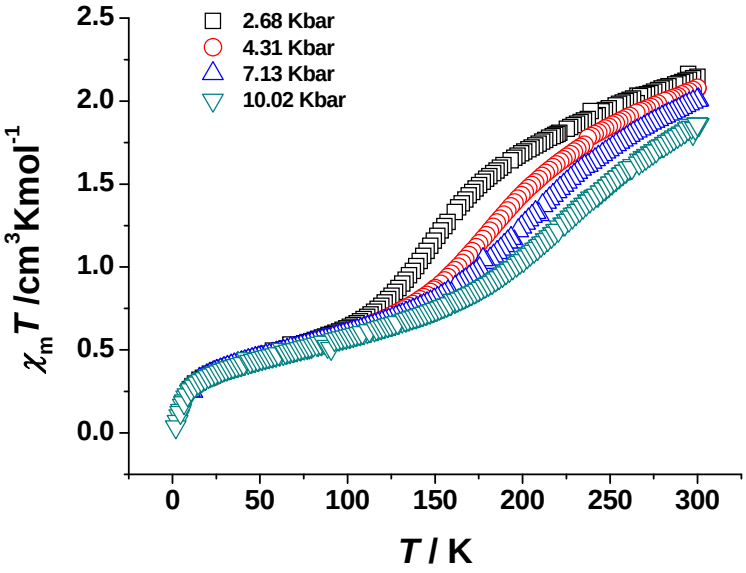

Figure S6. The temperature-dependent $\chi_M T$ at different pressures for **1**

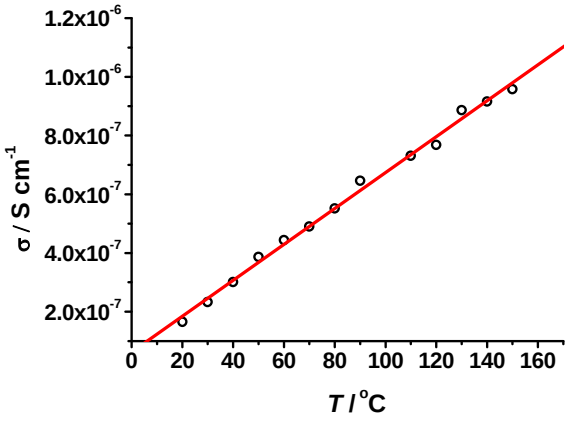

Figure S7. Temperature dependence of the electrical conductivity above room temperature for **1**.

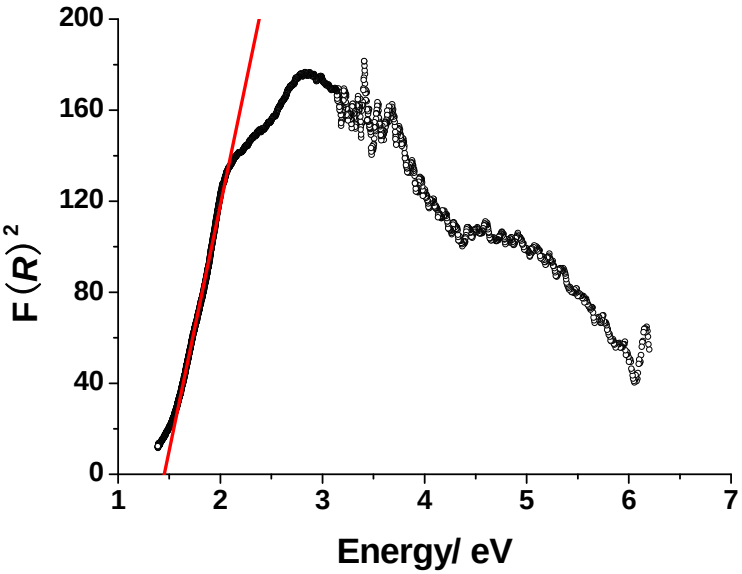

Figure S8. Optical absorption spectra of **1** at room temperature.

The UV absorption data were calculated from the reflectance data using the Kubelka-Munk Function of $\alpha/S = (1-R)^2/2R$, where R is the experimentally observed reflectance, α the coefficient and S the scattering coefficient.

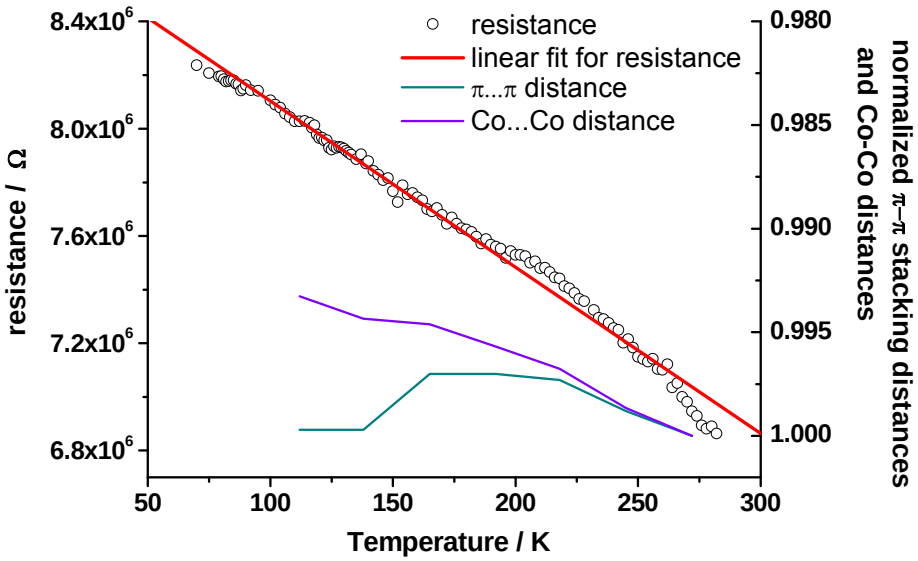

Figure S9. Temperature dependence of the resistance and normalized π–π stacking distances and/or the Co···Co distances for **1**.

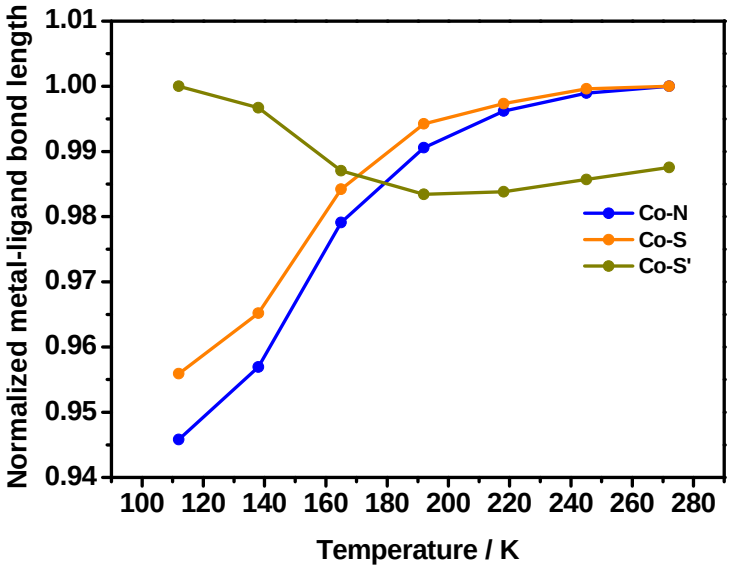

Figure S10. Temperature dependences of the coordination bond lengths normalized for **1**.